Research article

Control investigation of a customizable/adjustable exoskeleton upper-limb

Riaan Stopforth
Mechatronics and Robotics Research Group (MR2G) Bio-Engineering Unit, University of KwaZulu-Natal, Durban, South Africa

Abstract
Purpose – The purpose of this paper is to investigate the mechanical, kinematic and biological aspects that would be required for a customized upper limb exoskeleton prototype operation.
Design/methodology/approach – The research contained a literature survey, design, simulation, development and testing of an exoskeleton arm.
Findings – An adjustable/customizable exoskeleton arm was developed with a kinematic model to allow the desired motion. Tests were performed to determine the feasibility of the system.
Originality/value – The paper shows how the authors researched, designed and developed an exoskeleton arm that had similar mechanical properties to those of a biological arm. The exoskeleton must allow customization and be adaptable to the operator, without the need for major alterations.

Keywords Artificial limbs, Prototypes, Kinematics, Bio-mechatronics, Customizable, Exoskeleton arm, Kinematic model, Control

Paper type Research paper

1. Introduction

An exoskeleton arm is an external mechanical structure which has joints that correlates to the human arm. This integration allows for the transfer of mechanical power to the biological upper-limb (Panich, 2010). Exoskeletons can be classified into three categories, which allow humans to (Akdogan and Adli, 2011):

1 assist individuals with their daily activities;
2 support mobility; and
3 aid therapy by providing mobility and therapeutic exercise.

Safety, adjustability, functionality and portability are objectives that are considered for the exoskeleton arm. The customizability must be possible with minimal alterations within a minimal time period.

The different types of motion that occur in the three anatomical planes are: extension/flexion, abduction/adduction and supination/pronation. These terms are explained as (Pons, 2008):

1 Extension and flexion occur in the sagittal plane. Extension is movement in which the angle between the bones and body parts increase. Flexion is movement in which this angle reduces.
2 Abduction and adduction occur in the coronal plane. Abduction is the motion in which the angle between the bones and body parts increase. Adduction is movement in which this angle reduces which results in the bone being closer to the body.
3 Supination and pronation is the rotation of the forearm. Supination is rotation so that the palm faces upwards whereas pronation is rotation such that the palm faces downwards.

The robot-human interaction has been investigated with the Mitsubishi Pa10-7 robot to compare trajectories for rehabilitation of stroke victims (Caimmi *et al.*, 2012). Current upper-limb exoskeleton designs are mainly built for the purpose of haptic, tele-operations, rehabilitation and strength enhancement applications. Tele-operation is the process by which a slave robot is controlled, at a distance, via the replication of forces and movements performed by an operator using an exoskeleton arm (Bergamasco *et al.*, 1994). Haptic interface is the interaction of the exoskeleton and the operator through human touch which can be used to control virtual reality environments (Hayward *et al.*, 2004). Strength enhancement is implemented in exoskeleton devices to aid individuals in bearing or carrying large loads (Pratt *et al.*, 2004). A study conducted with patients on some of these exoskeleton designs was performed and it was found to improve their motor performance and decrease muscle spasticity (Frisoli *et al.*, 2012). Some of the current available upper-limb exoskeletons have incompliancy and lack adaptability with critical condition movements, such as the joint misalignment of the exoskeleton and human elbow joints (Malosio *et al.*, 2011).

Various exoskeleton arm designs were analyzed and the joint specifics of the MGA, MAHI, L-EXOS and the CADEN-7 exoskeletons were obtained to compare with human joint angles. The total range of motion of these exoskeletons was studied and tabulated in Table I, according to the joint movements. The tabulated values printed in red are joints that are capable of rotating more than the specific human joint can handle. This can cause severe damage, resulting in hyper

The current issue and full text archive of this journal is available at **www.emeraldinsight.com/0143-991X.htm**

Industrial Robot: An International Journal
40/2 (2013) 132–142

[DOI 10.1108/01439911311297739]

Table I Joint movement in degrees

	DOF	MGA (Carignan and Liszka, 2005)	L-EXOS[a] (Frisoli and Rocchi, 2005)	CADEN-7[a] (Perry and Rosen, 2006)	MAHI (Gupta and O'Malley, 2007)	HUMAN (Standard, 2009)	ADL (Perry and Rosen, 2006)
Elbow	Flexion	142	105	150	120	138	115[a]
Wrist	Supination/pronation	Not actuated	180	60	180	172	150[a]
Shoulder	Extension/flexion	210	135	180	–	236	110[a]
	Adduction/abduction	138	140	180	–	173.5	100[a]
	Lateral/medial	131	135	160	–	160	135[a]

Notes: [a]Values are mechanical joint capabilities for both directions (total) where applicable; [b]values are the 50th percentile of a test of 100 males; female joints are more flexible (Standard, 2009); [c]ADL – activities of daily living (Perry and Rosen, 2006)

extension or flexion of the human joints. Therefore, safety is an essential factor in this design and the proper implementation will be discussed further in this paper.

The term spherical motion, which is used often in this paper, refers to the motion of the shoulder in the desired workspace, without exceeding the limits that will cause discomfort or pain. All motions are controlled by the graphics user interface (GUI). It is also important to note that traditional exoskeletons consist of three mutually intersecting orthogonal joints which replicate the spherical motion of the shoulder joint, being the fundamental motion required to create a large workspace according to the activities of daily living (ADL) (Liszka, 2006). However, this orthogonal layout is undesirable as it results in a singularity in the workspace. A singularity is created when two joint axes become co-linear; any further rotation regarding the joints will yield the same result. This results in a loss of a degree of freedom (Ider, 2008). As a result the Jacobian, used in the kinematic model, reduces in rank and the subsequent matrix would command an infinite speed in the relative joint axes, which is not desired (Liszka, 2006). As the mechanical structure approaches a singularity, larger changes in joint angles result in smaller changes in the end-effecter position. This is the main reason why one cannot work around a singularity in the middle of the workspace because the structure will always be in close proximity of the singularity (Craig, 2005). A singularity cannot be removed from the mechanical design.

Other similar designs, as discussed in this paper, have been developed recently. The sensoric arm master (SAM) exoskeleton (Letier *et al.*, 2008) has been designed to eliminate singularities in the sagittal plane, while restricted in the transversal and coronal plane. The IntelliArm is an 8 + 2 DOF exoskeleton system for rehabilitation purposes (Ren *et al.*, 2009), but consists of a mechanical construction that prevents the ease of transportation.

For the objectives to be obtained, it was required to develop an exoskeleton that will allow for a three step process to occur with the customizability. The first step involves the measurement of different segments of the arm, which can be used for the dimensions of the exoskeleton. This distance is measured between the centers of the shoulder joint and elbow joint. The Next Engine 3D inspection Scanner converts 3D scans to parametric solid models that can be transferred to CAD models. The forward and inverse kinematic models rely on the dimension of the mechanical properties. The second stage will be to modify the mechanical segments while the third stage is to enter these dimensions within the system so that the error in control is minimized.

A bio-mechatronics system consists of the integration of the biological, mechanical, electronic and computer engineering research fields (Naidu *et al.*, 2012). The measuring of the upper-limbs is discussed, considering the bio-mechatronics integration. The mechanical design that was used for the motion of the shoulder, elbow and wrist joints is explained. The kinematic models that are used are given with tests that were performed. The system is to be easily transported, yet considering a low cost system. The upper-limb exoskeleton discussed in this paper was designed, to be used for rehabilitation purposes, and to assist disabled people with daily living activities involving the usage of their upper-limbs in the future. The exoskeleton upper-limb was to be designed to consider all possible motions, yet be simplified in terms of the mechanical design and kinematic control system.

2. Mechanical design

The biological arm consists of three main parts: the upper arm, the forearm and the hand which are connected together via three joints. The upper arm is connected to the trunk segment (torso) via the GH joint, which is commonly known as the shoulder joint. The forearm is connected to the upper arm via an elbow joint; and the hand is connected to the forearm via the wrist joint.

The DOF in the human biological arm can be imitated using seven mechanical DOF; these comprise of three DOF in the shoulder joint, two in the elbow joint and two in the wrist (Carignan and Liszka, 2005). The design of the exoskeleton arm had to cater for the majority of these motions in order to replicate the human workspace required to perform the ADL, as previously explained.

Different designs were considered for the shoulder. The design shown in Figure 1 was used, as the kinematic model allowed for simplification, while the required motion was possible.

Figure 1 3D CAD view of the shoulder concept

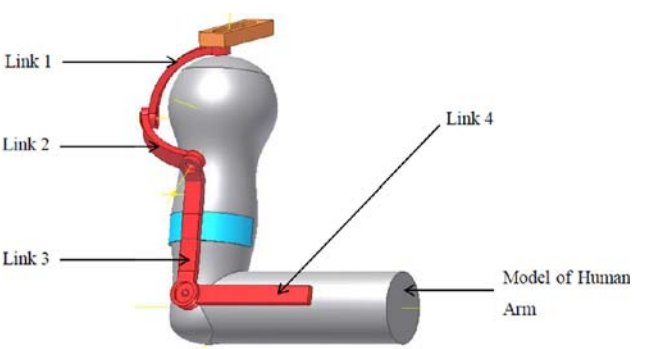

2.1 Adjustability

The angles between joints 1 and 2 and joints 2 and 3 are 75° and 90°, respectively. These joints were mutually intersected and were connected by curved links. This link layout allowed for a maximum user size of dimension according to the 95th percentile human being. The first shoulder joint was vertically above the GH joint, which is attached to the stand that supported the exoskeleton mechanism. Link 3, which joins the shoulder and elbow mechanisms, was made adjustable to accommodate various upper arm lengths up to the 95th percentile. This adjustability was easily achieved using a slot and two bolts with the two links sliding into each other. The carry angle adjustable mechanism was created by adding a joint in-between the link that connected joint three and the elbow joint (link three). This joint would effectively act as a hinge and would be fastened tightly at the desired position. The forearm (link 4) was also adjustable and was designed so that two lengths of square tubing could slide concentrically and be secured at the desired position.

2.2 Mechanical loading

A major inconvenience with a serial arrangement was that the entire load was endured by a single serial arm. Hence the moments/torques created by the exoskeleton and the upper-limb would propagate through the mechanical structure. Each joint and therefore motor experienced either a rotating torque or a bending moment that was created by the various loads acting along a moment arm. The orientation of the joints would determine whether the load would act as a joint rotation (torque rotation) or as a bending moment across the joint axis. The difference can be seen in Figure 2, between joint one and two. The greatest moments would be experienced when the arm was out stretched and flexed or abducted along the horizontal plane of the GH joint. Figure 2 shows that joint 1 would experience a bending moment across the joint axis, whereas joint 2 would encounter a torque load that would be endured by the actuator drive. The third and fourth joints would experience a combination of torque loads and bending moments because their axes were not orthogonal to the horizontal plane along which the upper-limb is positioned. This meant that the joints had to be designed to withstand both axial and radial loads as a result of the respective high torque and bending moments. These joints for this prototype system had to be designed and engineered to handle these loads.

2.3 The wrist mechanism

A number of conceptual designs were created and the spur gear concept was chosen. The spur C-gear rotates about an axis which was co-linear to the patients forearm. This common axis allowed for the transfer of mechanical power to the end-effecter which resulted in the supination and pronation movements. The final design consisted of a semi-circular gear which rotated within a slot about the co-linear axis. The C-gear was meshed with the pinion gear which provided a 5:1 gear ratio. This ratio was created for dimension purposes according to the 95th percentile being and not as a torque or speed requirement. The pinion gear was powered by a DC motor via a coupling and a keyway. The gears were encased in a gear cover which prevents exposure of the gear teeth and provided a mounting in which the forearm mechanism can be joined to the wrist mechanism via a U-tube. The pinion gear was designed to have an extended shaft which was supported by a ball bearing. This design minimized any load on the motor shaft which resulted in a minimal torque application, as the wrist mechanism only provided the rotational movement. This mechanism can be seen in Figure 3.

Figure 2 CAD illustrating the load on the joints, in worst case pose

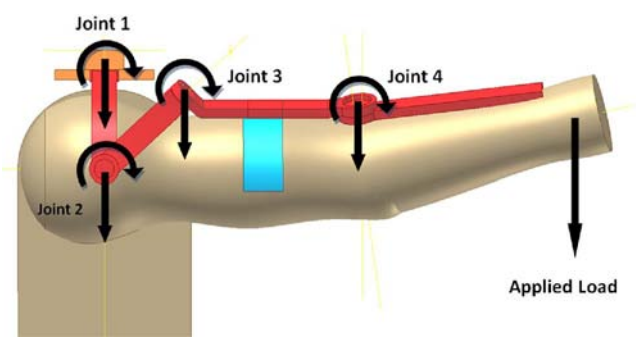

2.4 Material and development

Aluminum was used for the construction of the exoskeleton arm, due to its low weight characteristic, which is essential if a person or supporting structure has to carry the exoskeleton system. Once stress analysis was performed on the system, appropriate actuators were used for the joint motion. To prove the concept of this prototype, it had to lift a 2 kg weight. This low minimum requirement was to reduce the cost spent on the actuators. The Doga motors, that were considered for selection operates on 12 V, in order to be powered by a 12 V power supply. The torque, speed and weight of the motors were appropriate for the system, which was determined from the iterative calculations. Friction of the motor and the gearbox was included in the torque-speed curves provided by the manufacturer, allowing for the net torque values to be read from the curves.

The final shoulder and elbow mechanism is shown in Figure 4. The 90°, 75° and 45° angles represent θ_1, θ_2 and θ_3, respectively. Mechanical stops were also implemented into the design to stop motion past the limits of the ADL, to prevent the user from hurting themselves, should the control system fail.

The final construction of the system is shown in Figure 5.

Figure 3 Spur gear concept

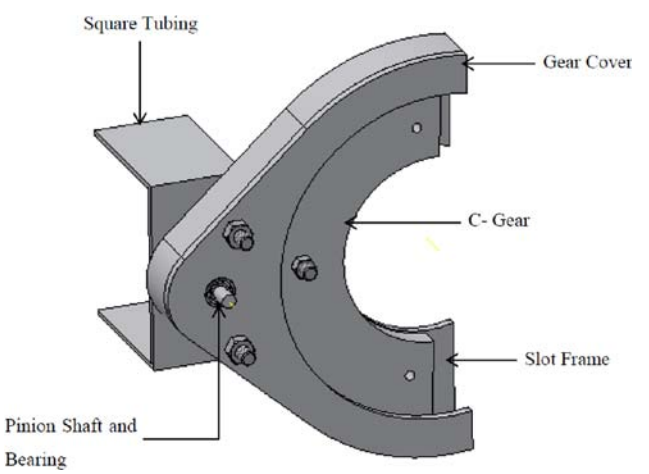

Figure 4 CAD of final shoulder and elbow mechanism

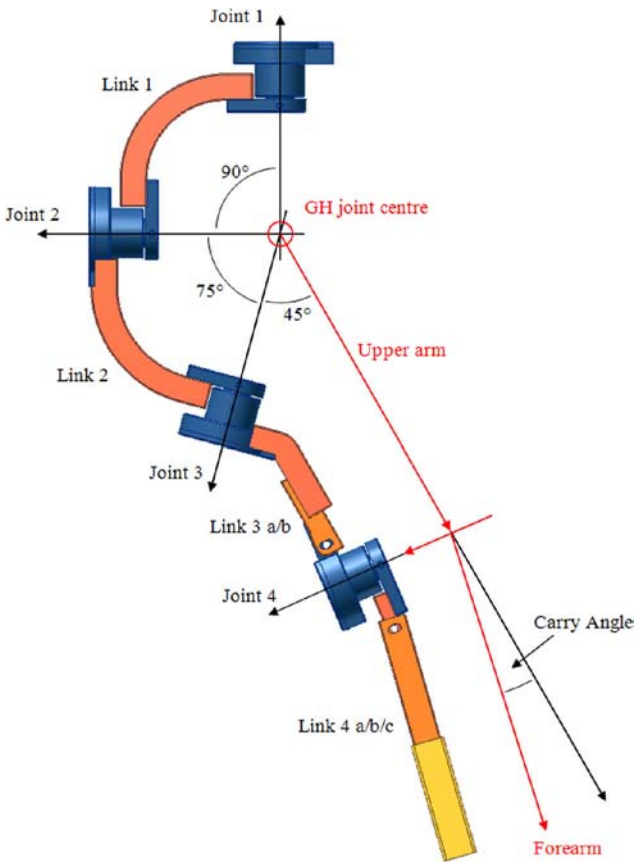

Figure 5 Final exoskeleton prototype mechanism with stand support

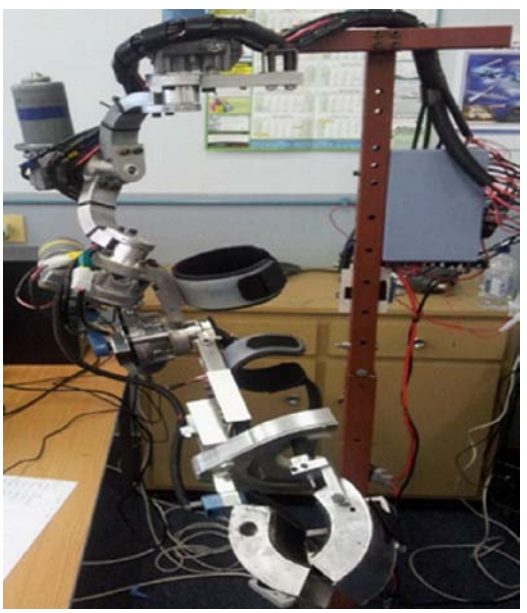

3. Customizable kinematic model

A simulation of the workspace and the position control during the user operation is dependent on the kinematic models. The Denavit-Hartenberg (DH) notation, which is the most common method used for manipulator kinematics (Craig, 2005), is used to derive the joint frames and transformation matrices. To solve the transformation matrices, the DH parameters had to be derived.

Table II shows the parameters according to the DH notation. ϑ_i represents the angle from X_{i-1} to X_i about Z_i (Craig, 2005). The transformation matrix of joint i relative to the previous joint is shown in equation (1) (Craig, 2005). The first three rows of column four within this equation are the X, Y and Z co-ordinates of joint i relative to joint i − 1, which will be used to solve the inverse kinematics. By substituting the tabulated parameters into equation (1), the individual joint transformations are obtained.

Where α_i, a_i, d_i and ϑ_i are the four DH parameters and represent the twist angle, link length, link offset and joint angles of joint i, respectively:

$$ {}^{i-1}_{i}T = \begin{bmatrix} c\vartheta_i & -s\vartheta_i & 0 & a_{i-1} \\ s\vartheta_i c\alpha_{i-1} & c\vartheta_i c\alpha_{i-1} & -s\alpha_{i-1} & -s\alpha_{i-1}d_i \\ s\vartheta_i s\alpha_{i-1} & c\vartheta_i s\alpha_{i-1} & c\alpha_{i-1} & c\alpha_{i-1}d_i \\ 0 & 0 & 0 & 1 \end{bmatrix} \quad (1) $$

Matrices 2-6 (Naidu *et al.*, 2011) represent the DH parameters. Sine (ϑ_1) and cosine (ϑ_1) are represented by s1 and c1, respectively. L1 represent the distance from the GH joint to the elbow joint while L2 indicates the length from the elbow joint to the center of the end-effector. L1 and L2 varies in length depending on the adjustability for customization for the user:

$$ {}^{0}_{1}T = \begin{bmatrix} c1 & -s1 & 0 & 0 \\ s1 & c1 & 0 & 0 \\ 0 & 0 & 1 & 0 \\ 0 & 0 & 0 & 1 \end{bmatrix} \quad (2) $$

$$ {}^{1}_{2}T = \begin{bmatrix} c2 & -s2 & 0 & 0 \\ 0 & 0 & 1 & 0 \\ -s2 & -c2 & 0 & 0 \\ 0 & 0 & 0 & 1 \end{bmatrix} \quad (3) $$

$$ {}^{2}_{3}T = \begin{bmatrix} c3 & -s3 & 0 & 0 \\ s3.c\frac{5\pi}{12} & c3.c\frac{5\pi}{12} & -s\frac{5\pi}{12} & -s\frac{5\pi}{12}.L1.\sqrt{2} \\ s3.s\frac{5\pi}{12} & c3.s\frac{5\pi}{12} & c\frac{5\pi}{12} & -c\frac{5\pi}{12}.L1.\sqrt{2} \\ 0 & 0 & 0 & 1 \end{bmatrix} \quad (4) $$

Table II DH parameters

i	α_{i-1}	a_{i-1}	d_i	ϑ_i
1	0	0	0	ϑ_1
2	$-\pi/2$	0	0	ϑ_2
3	$5\pi/12$	0	$L1.\sqrt{2}$	ϑ_3
4	$3\pi/4$	0	$L1$	ϑ_4
5	$-\pi/2$	0	$L2$	ϑ_5

$$ {}^{3}_{4}T = \begin{bmatrix} c4 & -s4 & 0 & 0 \\ s4.c\frac{3\pi}{4} & c4.c\frac{3\pi}{4} & -s\frac{3\pi}{4} & -s\frac{3\pi}{4}.L1 \\ s4.s\frac{3\pi}{4} & c4.s\frac{3\pi}{4} & c\frac{3\pi}{4} & -c\frac{3\pi}{4}.L1 \\ 0 & 0 & 0 & 1 \end{bmatrix} \quad (5) $$

$$ {}^{4}_{5}T = \begin{bmatrix} c5 & -s5 & 0 & 0 \\ 0 & 0 & 1 & L2 \\ -s5 & -c5 & 0 & 0 \\ 0 & 0 & 0 & 1 \end{bmatrix} \quad (6) $$

Equation (7) is obtained by matrix multiplication of matrices 2-6, which represents the transformation matrix of the end-effector relative to the base frame:

$$ {}^{0}_{5}T = {}^{0}_{1}T^{1}_{2}T^{2}_{3}T^{3}_{4}T^{4}_{5}T \quad (7) $$

The change in X, Y and Z for the combination of joint angle changes are determined by the forward kinematics, which allow for the generation of a simulation of the workspace. This simulation determines whether the shoulder is able to manoeuvre to the desired angle. By taking the joint constraints into consideration, the workspace is generated. ϑ_1, ϑ_2, ϑ_3, ϑ_4 and ϑ_5 are constrained to $-30°$ to $150°$, $-150°$ to $-30°$, $0°$ to $137°$, $0°$ to $120°$ and $0°$ to $175°$, respectively, according to the kinematic models.

Figure 6 shows the *x*- and *z*-axis of the mechanical manipulator. X_i was normal to Z_i and Z_{i+1}. X_i and Z_i were the joint frame axes of *joint*$_i$. The axes X0 and Z0, which were at the same initial position as X1 and Z1, represented the base axes. Y0 was obtained according to the right hand rule and pointed in the direction of X3 and X4 in Figure 6. The *z*-axes were also the respective joint's axis of rotation, and the intersection of a set of Z and *x*-axes is the origin of the respective joint. As shown in Figure 6, The X_i axes is in red intersecting corresponding Z_i axes. The transformation matrices consisted of θ_i which referred to the rotation from X_{i-1} to X_i about Z_i (Craig, 2005).

Figure 6 CAD of mechanical manipulator with respective *x*- and *z*-axes

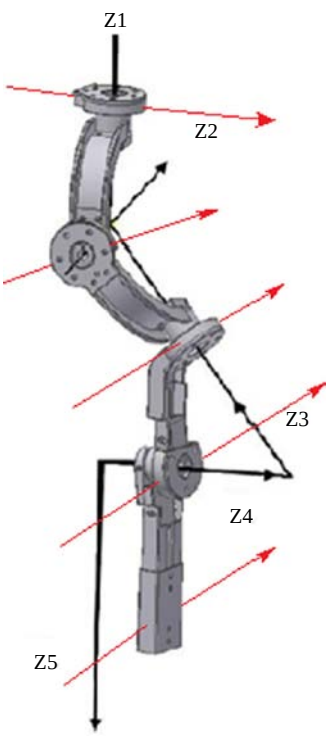

Note: The X_i axes is in red intersecting corresponding Z_i axes

For safety reasons, the joint constraints are implemented to prevent the collision of the mechanism with the user, link collision and hyper flexion or extension of the human joints. L1 and L2 were taken as 250 and 350 mm, respectively, for the simulation results conducted in Figure 7.

The workspace of the end-effector possesses a spherical nature which is inherent with the abilities of the shoulder mechanism. The workspace was generated by using the range of the minimum and maximum joint limits, incrementing joints 1-3's angles by 20°, while joint 4's angles were incremented by 10°. The results of this workspace allows for a feasible inverse kinematics calculation.

The angles between joints 2 and 3 and joints 3 and 4 are 75° and 135°, respectively. The result of a complex algebraic inverse solution is due to the number of non-zero terms within the transformation matrices. The non-orthogonal layout produces a difficult geometric solution which is further coupled by a 3D problem (Na *et al.*, 2008). From several inverse kinematic iterative methods, the damped least squares (DLS) method is the best method when dealing with singularities and complex designs (Buss, 2004). The DLS method implements the Jacobian of the positional vector of the mechanism and is required to solve the change in ϑ_i. The calculations and implementation of the inverse kinematics for the system is explained by Buss (2004).

The algorithm that was implemented with the upper-limb exoskeleton, using the DLS method, is shown in Figure 8. The error that was initially calculated was used to solve the angle change. After updating the error values and the joint angles, the process is repeated until the error value is acceptable.

Figure 7 Workspace of the exoskeleton mechanism which results in a spherical motion

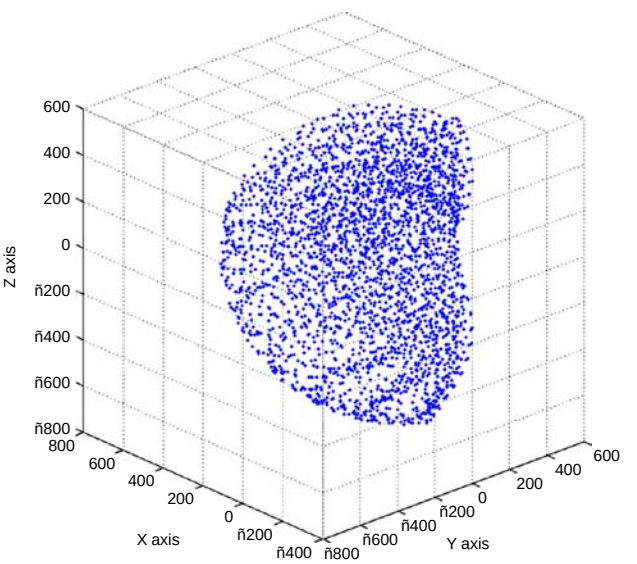

Figure 8 Flowchart illustrating the iteration process of the DLS method

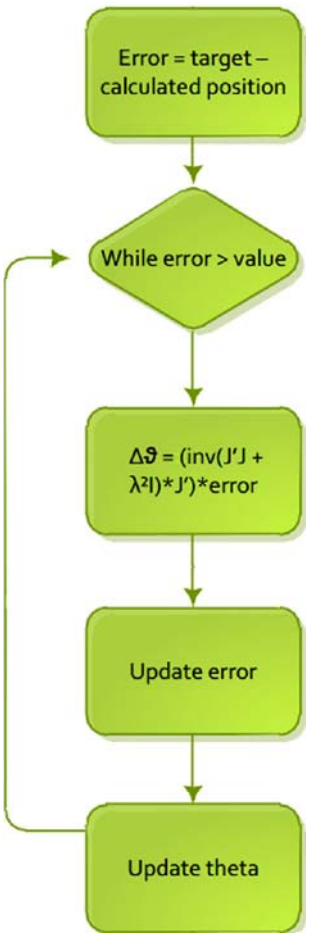

4. Tests and results

Figure 9 shows a basic interaction of the system with the PC. The solid blue lines indicate the power lines and the solid red lines indicate the direction of the electronic signal flow.

The microcontroller that was used is the ATMEGA 1280. A PC was used to send instructions to the microcontroller and to obtain the feedback results from the exoskeleton system, to determine the error that might occur. Safety switches were also connected to the microcontroller, to prevent motion past the human or mechanical limits of the exoskeleton, should the control system fail. With the kinematic models that were derived previously, it was possible to perform tests by entering the joint angles, or the (X Y Z) co-ordinates with reference to the frame of the exoskeleton. The two servos were used to mimic the motion of a gripper at the end of the exoskeleton arm, allowing for such a feature should it be required. The robotics communication protocol (RCP) (Stopforth *et al.*, 2011) was used for the communication between the PC and the exoskeleton.

Impedance control is the control of a mechanical system that incorporates force and motion. Impedance control theory relates to the motion of a human's limb, but the system has to be tuned intuitively by the designer for each individual. To overcome this time consuming problem, the system could learn the different characteristics of the individual user, incorporating an adaptive-related control system (Suzuki and Furuta, 2012). Since the prototype exoskeleton was developed for the mentioned objectives, it was decided to use PID control to test the system. Future work would allow for the implementation of impedance and adaptive control methods.

PID theory reveals that the proportional gain would have the effect of reducing the rise time, which was the time it took to go from the initial to the reference value. This gain would also reduce the steady state error which was the difference between the input and output values (the tracking error). The initial pulse width modulation (PWM) is not large enough to create a movement against a load. The integral wind-up allowed for the PWM to increase in a stationary system which would increase the chances of motion in a high load operation. The derivative gain could improve the systems stability, transient response and reduce overshoot. It was therefore decided to investigate the different gains and their impact on the responses. The responses were analyzed according to the iteration count (number of loops) and not according to time, as this allowed for better observation of the looping structure.

The proportional term was investigated for different values and their responses are plotted in Figure 10. The steady state error was not completely eliminated as noticed in Figure 10.

Figure 11 shows the different K_i values that were plotted for a K_p of 5. It was noticed that the transient response was affected by the oscillations, and that the steady states errors were eliminated (except for $K_i = 0.1$).

Figure 9 Interaction of the actuation control module with the PC

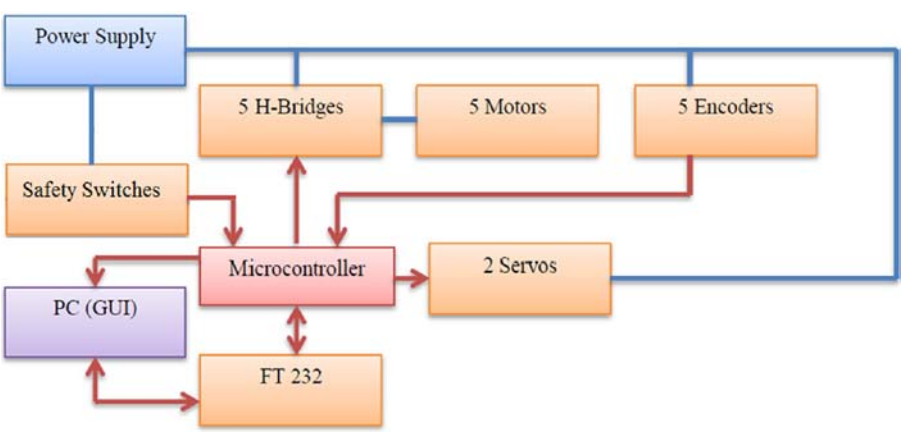

Figure 10 Proportional control gain values tested for the exoskeleton arm

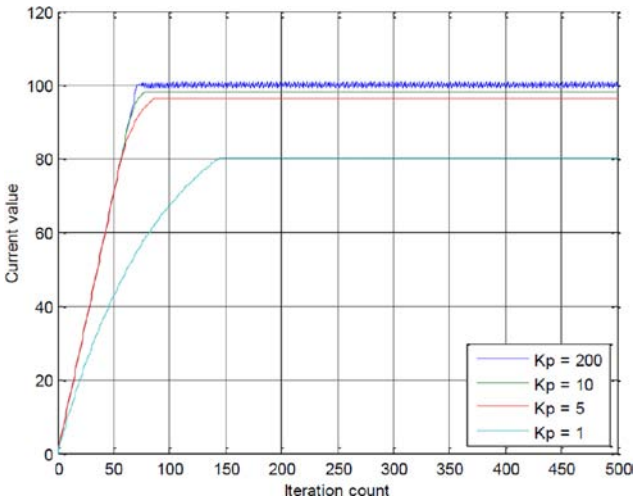

Figure 11 Graph representing the different responses for different Ki gains

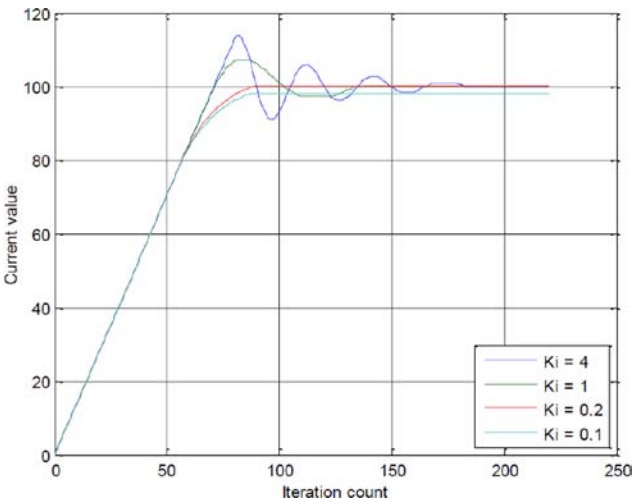

Note: Kp = 5

Figure 12 shows the different responses for different K_d values with a constant K_p and K_i of 5 and 0.2, respectively. The derivative gain increased the curvature of the step response and reduced the response before settling which was for a negative derivative gain. This curvature can be seen in Figure 12.

Gains were then chosen in order to give a smooth stable response without the need of a rapid response. The chosen step response is shown in Figure 13. This response is for K_p, K_i and K_d of 1.5, 0.2 and -20, respectively. The proportional gain was decreased from 5 as it provided a larger curved and hence a smoother step response.

The practical testing of the control system was illustrated in this chapter in order to express the implementation of the system in a more conclusive approach. The actual practical step response of the PID controller was compared to the theoretical step response in Figure 14. The experimental line was more jagged which is due to the fact that the encoder resolution was accurate to a degree and not to fractions of a degree. The practical response closely matched the theoretical response.

Figure 12 Graph representing the different responses for different K_d gains

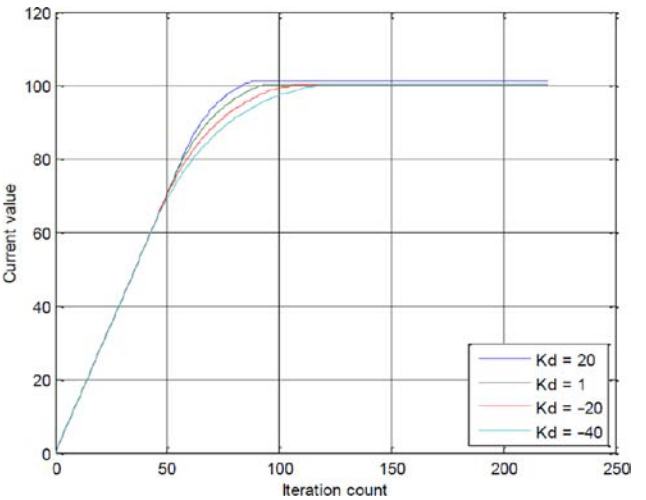

Notes: Kp = 5 ; Ki = 0.2

Figure 13 Graph illustrating the chosen PID response

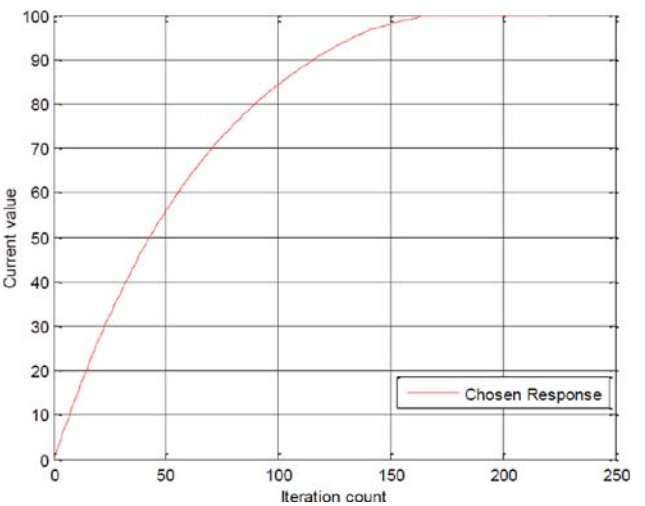

Figure 14 Graph comparing the PID theoretical and practical responses

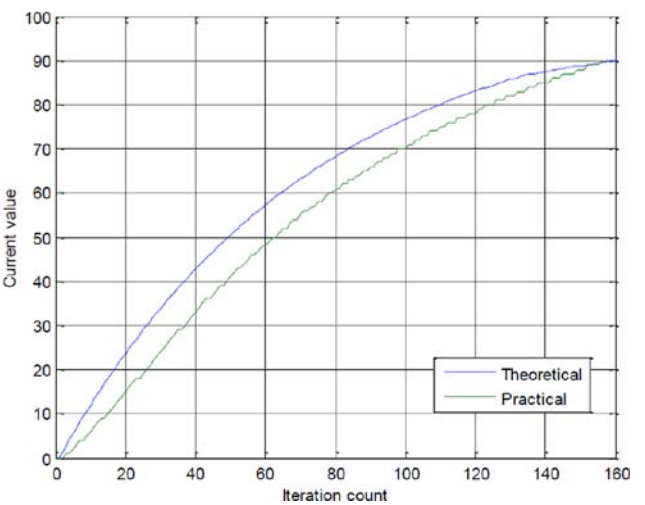

The slight offset in the responses could be as a result of the theoretical relationship between the PWM and the current value as compared to the practical encoder readings. Both responses resulted in stability and an elimination of the steady state error with no overshoot, which is as desired. However, the response on the initial movement was jerky. This was a result of the step response which supplied a high initial PWM for large error values.

This jerky motion was overcome by implementing a ramp input which increased linearly with every successive loop. This comparison is shown in Figure 15. The initial gradient of the ramp response is much less than that of the step response which resulted in a smoother control system. The ramp response resulted in a control system that consists of no overshoot, no steady state error and was stable and smooth. Therefore, the ramp response was implemented as the control system that provided the required passive motion. The derivative gain was not implemented in the ramp response. The ramp input incremented by a value of one for every successive loop. This small resolution required no additional damping, therefore a PI ramp controller was implemented.

Position tests were performed as shown in Figure 16.

Tests have shown that after 140 interactions, the angle and position is achieved. This is seen in Figure 17.

A load of 1 kg was placed on the end of the elbow mechanism, link 4. The elbow was fully extended and only the shoulder mechanism was mobilized to produce the worst case pose for the prototype system. The load was repeatedly incremented by 1 kg until a load of 5 kg was achieved and the shoulder mechanism repeatedly moved from the anatomical position to the worst case pose. The elbow mechanism was tested by moving the elbow from the anatomical position to 90° of flexion. This test was repeated for 1-5 kg with an increment of 1 kg during each test. These tests proved that the exoskeleton arm was able to lift a 2 kg object. The tests were conducted with weights up to 5 kg, to determine if a safety factor was available on the system. The increase of the weight was also conducted to determine if the exoskeleton would fail if higher loads were applied to the system. These loads could be due to different weights of the user's arms that will be lifted. Photographs of the shoulder test at the worst case pose with a 5 kg load can be seen Figure 18. The elbow test with a 5 kg weight is shown in Figure 19.

Figure 15 Graph comparison between the step and ramp response

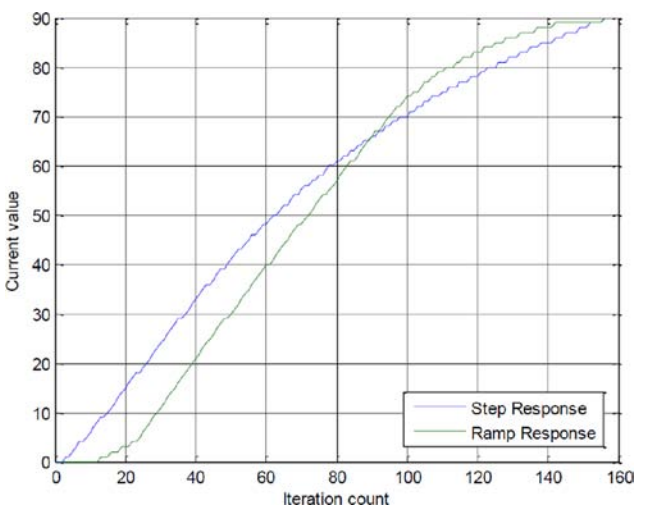

Figure 16 Position tests being performed

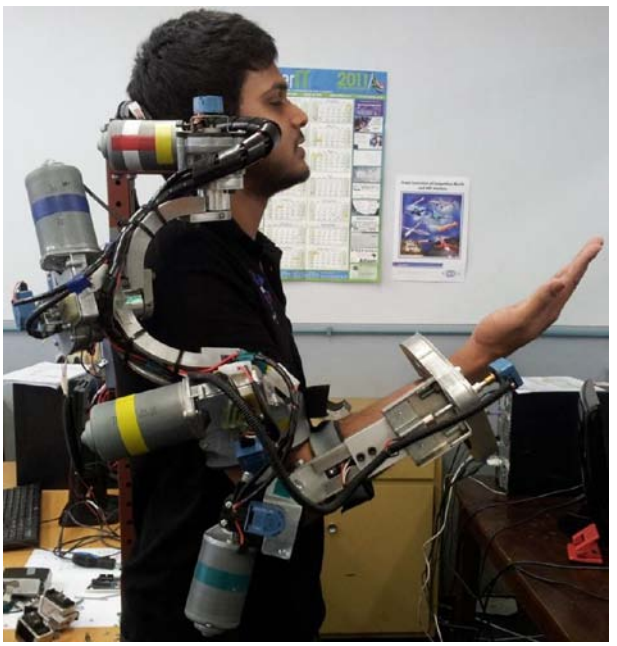

The time to lift the different weights by the different joints was recorded. A linear relationship is observed, as the time increased as the mass increased. The shoulder and elbow joint's results are observed in Figures 20 and 21, respectively.

The wrist mechanism was tested to rotate various loads which were acting against its rotation. The C-gear was rotated 90° such that the C gear was positioned above its horizontal axis, which resulted in the load acting against the rotation. Loads ranging from just the weight of the C-gear up to 2 kg were timed and a trend line was produced as executed with joints 2 and 4. The time and mass relationship is observed to be linear as shown in Figure 22. A maximum weight of 2 kg was tested on the wrist joint, as this was the maximum proposed weight that would be expected past the wrist joint.

The workspace of the exoskeleton manipulator was larger than that of the ADL. The shoulder rotation was 3.7 percent lower than the desired value, however this was acceptable. Load tests on the shoulder and elbow mechanism were conducted. These tests were done for a load of 5 kg without any noticeable heating to any of the components. The stall requirements according to the normal operation human isometric strength (HIS) specifications were satisfied. The wrist mechanism was capable of moving a 2 kg direct load without any signs of stalling, resulting in a linear relationship between time and mass. The inverse kinematic model was tested and an accuracy of 88.7 percent was achieved. Encoder counts were statistically analyzed and errors were detected. These errors could be the result of position; however future investigations need to be executed. A ramp PI controller was created producing a smoother response.

5. Conclusion

A customized exoskeleton prototype mechanism was designed to consist of a five DOF manipulator with a two DOF end-effecter. The shoulder and elbow mechanism was of higher priority as these were the mechanisms that affected the positional task space of the mechanism relative to the workspace environment. A spherical motion was required in order to

Figure 17 Correction in the position value (left) and the angles (right) are achieved after 140 iterations

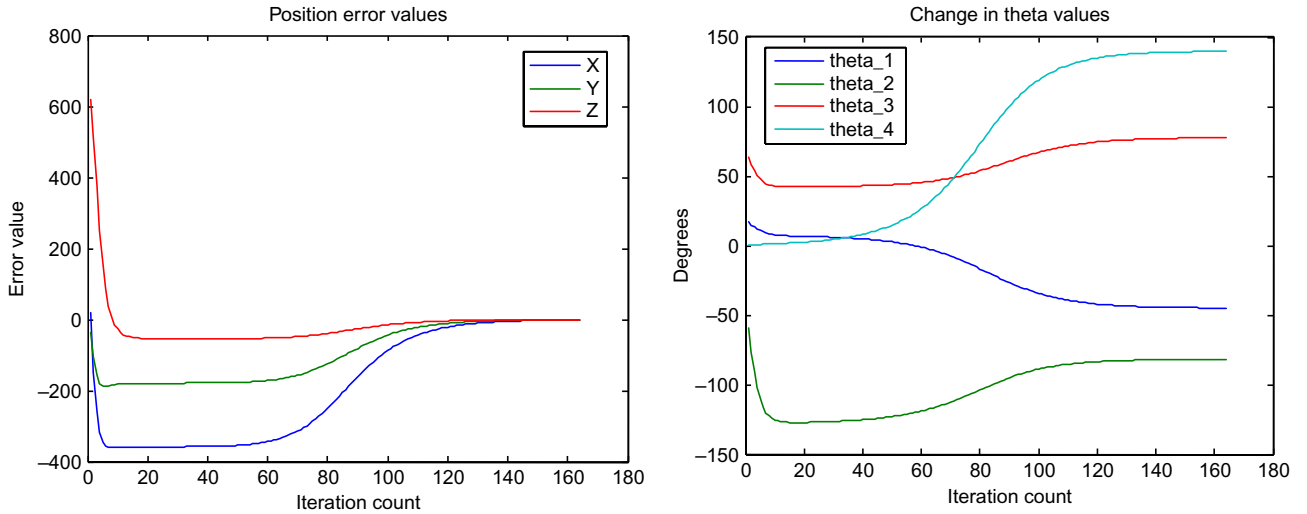

Figure 18 Shoulder flexion of 5 kg mass

Figure 19 Elbow flexion of 5 kg mass

imitate the workspace of the GH joint. A spherical workspace was generally achieved by three serial-orthogonal, mutually-intersecting joints. This layout resulted in a singularity in the human workspace that hindered motion. Movement of a singularity was achieved by the change in joint orientation however this affected the workspace of the mechanism. The exoskeleton manipulator was designed to be less than 10 kg, allowing it to be portable and adjustable.

Forward kinematics of the mechanism was derived using the DH notation. This method required the setup of individual joint axes which was required to determine the DH parameters. These parameters were used to solve the relative joint-transformation matrices which were mathematically computed to produce the forward kinematics. This kinematic model was used to determine the spherical workspace of the design. The change in the non-orthogonal layout resulted in extensive forward kinematics. This change

Figure 20 Graph of time vs mass for the shoulder joint

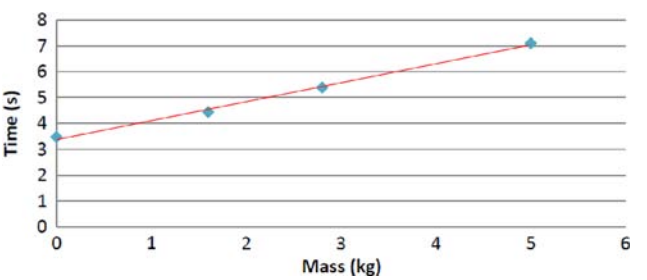

Figure 21 Graph of time vs mass for the elbow joint

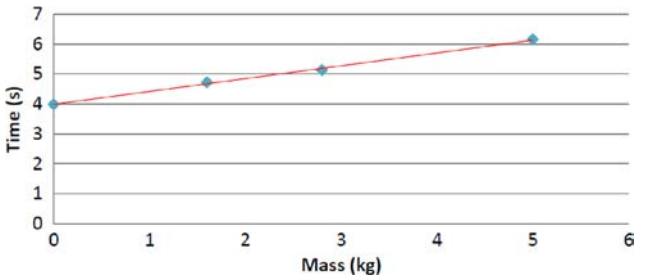

Figure 22 Graph of time vs mass for the wrist motor

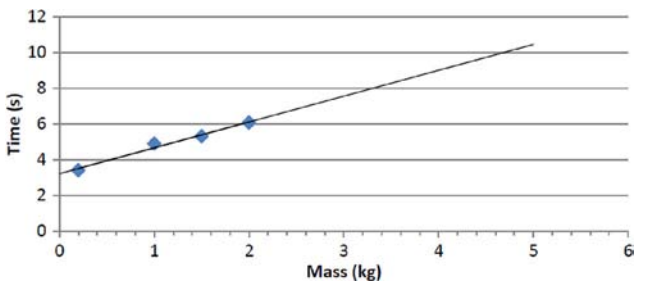

complicated the inverse kinematics problem which could not be solved algebraically or geometrically as this problem was further complicated by its 3D nature. The solution to the inverse kinematics problem was obtained iteratively via the DLS method. This iterative solution may prove useful in future developments as it could be implemented in obstacle avoidance. A redundant and non-redundant kinematic model was created. A joint limitation technique was implemented in both the redundant and non-redundant model. This implementation resulted in the Joint Limited DLS method in a redundant system. The non-redundant model allowed for a larger workspace and for separate control of the shoulder mechanism. A linear derivation of the inverse kinematics was illustrated through kinematic trajectories. Change in position was plotted against iteration count and it proved to stabilize as the error approached zero. This change in position was dependent on the initial position. The inverse kinematics model produced minimal error which was achieved by sending the inverse kinematic results into the forward kinematic model.

PID control was implemented as discussed in this paper. The results were satisfactory for the given K_x values (which were achieved by trial and error), that were used within the control algorithm. Problems that could occur with the use of PID control, is that the K_x values would need to be altered for different arm weights and therefore an adaptive control algorithm would be desired. Similarly, the control algorithm will be affected by the mechanical arm forces and motion that will be acting on the system, therefore an impedance control algorithm would also be desired. Impedance control would still be required to be tuned for each individual user. Due to the integration of the two desired control algorithm, an adaptive-impedance control system should be considered that will allow for a better performance of human-machine interaction.

A workspace test was achieved by driving the exoskeleton to the limits of each of its joints (limited by mechanical stops). The combined workspace was larger than the workspace of the ADL with the shoulder rotation not achieving 3.7 percent of the desired motion in that joint alone. Load tests on the shoulder, elbow and wrist mechanism were carried out. The shoulder and elbow mechanism lifted loads that produced approximately 1/4 of the HIS without the motors demonstrating any signs of stalling during normal operation. During the tests none of the fuses were damaged and there was no noticeable heating amongst the components of the design. The load tests on the wrist mechanism produced a linear mass-time relationship. The wrist rotational motion was approximately 6 s for a 90° rotation. Although this motion was slow, it was still acceptable as it provided passive therapy which would assist reducing spasticity of the joint. The hand mechanism provided the required gripping motion and propagated the wrist rotation, however future developments must consider a more compact design. An empirical measurement was done in order to measure the inverse kinematic model. This measurement yielded an error of 11.3 percent. This error could be as a result of the encoder resolution being rounded off during the calculations and the mechanical manufacturing errors. These errors need to be investigated in future development in order to provide a physiotherapeutic exoskeleton device.

The operation of the biological arm and previous exoskeletons were researched. The mechanism was designed and developed such that the exoskeleton had similar mechanical properties to those of the biological arm. This research, design and development met the research objectives specified in the introduction. The electronic components were researched and the complete electronic layout was developed. The safety specification was achieved through mechanical, electronic and software implementations. The workspace of the mechanism was analyzed, which achieved a combinational workspace that is better than that of the ADL. The workspace and load tests resulted in achieving the functionality aspects required.

The discussed exoskeleton has been developed considering a low cost factor. The weight of the exoskeleton manipulator was 9.3 kg which was below the specified weight. With the specific weight, it allows the exoskeleton to be transported, making it possible for a person to be rehabilitated at remote locations where the health sector is poor. The exoskeleton allows for future work to be conducted for other applications, as discussed in the future work section.

5.1 Future work

The motors that were used to validate the prototype system had a minimal torque, allowing for a maximum lifting weight of 5 kg and a wrist rotation of 2 kg. The use of higher torque motors that have a low weight ratio, would be more beneficial for heavier weights, but would increase the cost. These motors will be dependent on the type of application and the weight that is expected to be lifted by the exoskeleton arm. Adaptive-impedance control systems could be investigated that will allow for a better performance for human-machine interaction.

The discussed exoskeleton has future applications to allow disabled people the functionality of using their upper-limbs. The control of the exoskeleton system will be by means of an electroencephalography (EEG) or implanted electrodes. Although the 10 kg weight will be heavy for a disabled person to wear, it will be possible to use the exoskeleton with additional support. A disabled person that has spinal injuries has the inability to either their arms or legs or both. The designed exoskeleton will therefore have the ability to be supported by either a lower-limb exoskeleton system, or it could be mounted onto a wheelchair to aid the disabled person.

References

Akdogan, E. and Adli, M.A. (2011), "The design and control of a therapeutic exercise robot for lower limb rehabilitation: physiotherabot", *Mechatronics*, Vol. 21, pp. 509-22.

Bergamasco, M., Allotta, B., Bosio, L., Ferreti, L., Parrini, G., Prisco, G.M., Salsedo, F. and Sartini, G. (1994), "An arm exoskeleton system for teleoperation and virtual environments applications", *IEEE*, Vol. 2, pp. 1449-54.

Buss, S.R. (2004), "Introduction to inverse kinematics with jacobian transpose, pseudoinverse and damped least squares methods", *IEEE Journal of Robotics and Automation*, 17 April.

Caimmi, M., Malosio, M., Pedrocchi, N., Vincentini, F. and Molinari, L. (2012), "Robot assisted training: the impact of trajectories and velocities on the subject's perception of the movement", *Gait and Posture*, Vol. 35, April, pp. S27-8.

Carignan, C. and Liszka, M. (2005), "Design of an arm exoskeleton with scapula motion for shoulder rehabilitation", *IEEE Conference on Advanced Robotics*, pp. 524-31.

Craig, J.J. (2005), *Introduction to Robotics – Mechanics and Control*, 3rd ed., Prentice-Hall, Upper Saddle River, NJ.

Frisoli, A. and Rocchi, F. (2005), "A new force-feedback arm exoskeleton for haptic interaction in virtual environments", *IEEE Proceedings of the First Joint Eurohaptics Conference and Symposium on Haptic Interfaces for Virtual Environment and Teleoperator Systems*.

Frisoli, A., Procopio, C., Chisari, C., Creatini, I., Bonfiglio, L., Bergamasco, M., Rossi, B. and Carboncini, M.C. (2012), "Positive effect of robotic exoskeleton trainin of upper limb reaching movemnets after stroke", *Journal of NeuroEngineering and Rehabilitation*, Vol. 9, June, Article 36.

Gupta, A. and O'Malley, M.K. (2007), "Robotic exoskeletons for upper extremity rehabilitation", in Kommu, S.S. (Ed.), *Rehabilitation Robotics*, InTech, Vienna, August, pp. 371-96.

Hayward, V., Oliver, R.A., Cruz-Hernandez, M., Grant, D. and Robles-de-la-Torre, G. (2004), "Haptic interfaces and devices", *Sensor Review*, Vol. 24 No. 1, pp. 16-29.

Ider, S.K. (2008), "Singularity robust inverse dynamics of parallel manipulators", in Ryu, J.-H. (Ed.), *Parallel Manipulators, New Developments*, InTech, Vienna, April, pp. 373-90.

Letier, P., Avraam, M., Veillerette, S., Horodinca, M., De Bartolomei, M., Schiele, A. and Preumont, A. (2008), "SAM: A 7-DOF portable arm exoskeleton with local joint control", *2008 IEEE/RSJ International Conference on Intelligent Robots and Systems, Nice, France*, pp. 3501-6.

Liszka, M. (2006), "Mechanical design of a robotic arm exoskeleton for shoulder rehabilitation", thesis, University of Maryland, College Park, MD.

Malosio, M., Pedrocchi, N., Vicentini, F. and Tosatti, L.M. (2011), "Analysis of elbow-joints misalignment in upper-limb exoskeleton", *IEEE International Conference on Rehabilitation Robotics*, Art. no. 5975393.

Na, M., Yang, B. and Jia, P. (2008), "Improved damped least squares solution with joint limits, joint weights and comfortable criteria for controlling human-like figures", *IEEE Conference on Robotics, Automation and Mechatronics*, pp. 1090-5.

Naidu, D., Stopforth, R., Bright, G. and Davrajh, S. (2011), "A 7 DOF exoskeleton arm: shoulder, elbow, wrist and hand mechanism for assistance to upper limb disabled individuals", *AFRICON, 2011, Livingstone, Zambia, IEEE, 13-15 September*, pp. 1-6.

Naidu, D., Stopforth, R., Davrajh, S. and Bright, G. (2012), "A portable passive physiotherapeutic exoskeleton", *International Journal of Advanced Robotic Systems*, Vol. 9.

Panich, S. (2010), "Kinematic analysis of exoskeleton suit for human arm", *Journal of Computer Science*, Vol. 6, pp. 1272-5.

Perry, J.C. and Rosen, A.J. (2006), "Design of a 7 degree of freedom upper-limb powered exoskeleton", *Proceedings of the 2006 BioRob Conference, Pisa, Italy, February.*

Pons, J.L. (2008), *Wearable Robots: Biomechatronic Exoskeletons*, Wiley, Chichester.

Pratt, J.E., Krupp, B.T., Morse, C.J. and Collins, S.H. (2004), "The Roboknee: an exoskeleton for enhancing strength and endurance during walking", paper presented at the International Conference on Robotics and Automation, New Orleans, LA.

Ren, Y., Park, Y.-S. and Zhang, L.-Q. (2009), "Developing a whole-arm exoskeleton robot with hand opening and closing mechanism for upper limb stroke rehabilitation", *IEEE 11th International Conference on Rehabilitation Robotics, Japan, June*, pp. 761-5.

Standard, A.N. (2009), *Human Factors Engineering – Design of Medical Devices*, Association for the Advancement of Medical Instrumentation, Arlington, VA.

Stopforth, R., Bright, G., Davrajh, S. and Walker, A. (2011), "Improved communication between manufacturing robots", *South African Journal of Industrial Engineering*, Vol. 22, pp. 99-107.

Suzuki, S. and Furuta, K. (2012), "Adaptive impedance control to enhance human skill on a haptic interface system", *Journal of Control Science and Engineering*, Vol. 2012, p. 10 (Article ID 365067).

About the author

Riaan Stopforth obtained BSc Eng (Electronics), MSc (Computer Science) and PhD Eng (Mechanical-Mechatronics) degrees from the University of KwaZulu-Natal (UKZN). He heads the Mechatronics and Robotics Research Group Search & Rescue Division and Bio-Engineering Unit at UKZN. His interests are in radio communication, mechatronics, robotics and bio-engineering. Riaan Stopforth can be contacted at: stopforth@ukzn.ac.za